Journal of Hydrology 660 (2025) 133395

Contents lists available at ScienceDirect

Journal of Hydrology

journal homepage: www.elsevier.com/locate/jhydrol

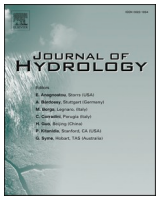

Research papers

Model based quantification of salinization dynamics under changing hydrological conditions in the Volturno River (Italy) coastal aquifer

Mattia Gaiolini [a], Abraham Ofori [a], Matteo Postacchini [b], Micòl Mastrocicco [c], Nicolò Colombani [a,*]

[a] Department of Materials, Environmental Sciences and Urban Planning, Polytechnic University of Marche, Via Brecce Bianche 12, 60131 Ancona, Italy
[b] Department of Civil and Building Engineering, and Architecture, Polytechnic University of Marche, 60131 Ancona, Italy
[c] Department of Environmental, Biological and Pharmaceutical Sciences and Technologies, Campania University "Luigi Vanvitelli", Via Vivaldi 43, 81100 Caserta, Italy

ARTICLE INFO

This manuscript was handled by Dongmei Han, Editor-in-Chief, with the assistance of Ryan T. Bailey, Associate Editor

Keywords:
Groundwater salinization
SEAWAT
HEC-RAS
Seawater intrusion
Paleo salinity

ABSTRACT

This work presents a semi-coupled modelling approach to study salinization dynamics in the Volturno River coastal aquifer (Italy), distinguishing among different salinization mechanisms. The area is of particular interest, given its location in the Mediterranean region, a climate change hot-spot. A 1D HEC-RAS numerical model was built up and run for a decade (2010–2020) to quantify the areal extent and timing of salinization events due to seawater encroachment within the Volturno River mouth. The results were used as input in a 3D SEAWAT model that incorporated salinity variations on a monthly basis for the same period. The SEAWAT model was down-scaled from a large calibrated MODFLOW model of the whole Campania region. Both national and worldwide databases were used to constrain the models. The model was then compared with 9 high resolution vertical profiles of porewater salinity obtained using a continuous coring sediment sampler, providing good model performance indicators (R^2 = 0.867, NSE = 0.808, and RMSE = 3.926 g/L). Results highlight an increasing groundwater salinization pattern due to intrusion from the Volturno riverbed. The classical mechanism of seawater wedge intrusion from the coastline was minimal, while large inland portions of the model domain were characterized by high salinity (up to 75 g/l) due to remnant paleo seawater trapped into peaty and silty-clay aquitards. This physically-based modelling approach could be replicated in any coastal porous aquifer (if hydrological and hydrogeological datasets are available) to identify and quantify the salinization mechanisms and to help water managers to implement tailored solutions in the most affected areas.

1. Introduction

Groundwater salinization is considered one of the major causes of freshwater resources deterioration in aquifers worldwide (Vengosh et al., 2003; Klassen and Allen, 2017; Parizi et al., 2019; Li et al., 2020; Mastrocicco and Colombani, 2021). This phenomenon is particularly pronounced in semi-arid zones and deltaic areas where groundwater pumping and climate change (CC) are likely to affect groundwater resources, potentially initiating or worsening salinization processes (Vaux, 2011; Aeschbach-Hertig and Gleeson, 2012; Parisi et al., 2018; Eswar et al., 2021; Richardson et al., 2024). In coastal floodplains, current seawater intrusion (SWI) is often pointed out as the main cause of groundwater salinization. Besides the classical direct seawater wedge from the coast, rivers and drainage canals can serve as preferential pathways for saltwater to migrate inland, thereby altering groundwater salinization dynamics (Ferguson and Gleeson, 2012; Hussain et al., 2019; Tully et al., 2019; Cao et al., 2020; Gaiolini et al., 2023). Additionally, recent studies targeted paleo-seawater as a foremost concern in many low-lying deltaic areas reflecting the complex evolution of marine transgressions and regressions during the Holocene (Colombani et al., 2017; Giambastiani et al., 2021; Dang et al., 2022; Alessandrino et al., 2023; Schiavo et al., 2023; Seibert et al., 2023; Yu et al., 2023). To boost a cost-effective management of groundwater resources, it is crucial to differentiate among these diverse salinization mechanisms gaining a deep comprehension of the complex interplay between freshwater and saline water. Quantifying the magnitude and spatial distribution of groundwater salinization is a fundamental but not easy task (de Louw et al., 2010). In addressing these challenges, the scientific community often rely on monitoring networks and numerical models to record and simulate the evolution of hydrogeological parameters in time and space.

* Corresponding author.
E-mail address: n.colombani@univpm.it (N. Colombani).

https://doi.org/10.1016/j.jhydrol.2025.133395
Received 25 October 2024; Received in revised form 13 April 2025; Accepted 26 April 2025
Available online 30 April 2025

To simulate SWI numerically and track the movement and evolution of the transition zone between fresh and saltwater, groundwater flow models that allow for a density-dependent simulation are necessary (Lu et al., 2013; Kourgialas et al., 2016). Various models, such as SUTRA, FEFLOW, and SEAWAT aid in forecasting groundwater dynamics and contaminant pathways addressing both groundwater-flow and mass transport equations (Bear and Cheng, 2010; Anderson et al., 2015) and many applications can be found in recent literature: Lyu et al. (2024) proposed a novel combined GALDIT and SEAWAT simulation method for dynamically predicting and evaluating vulnerability of coastal aquifer to seawater intrusion; in the same year an integrated FEFLOW-Python code was developed by Kassem et al. (2024) to optimize hydraulic barriers for mitigating seawater intrusion.

Models such as MIKE, Delft-3D, HEC-RAS, EFDC, and TUFLOW are widely used to simulate changes in surface water quality and are important for environmental management purposes (Pappenberger et al., 2005; Ji, 2017; Dingle et al., 2020). Among the most recent applications to manage salinity issues: the study of Soudi et al. (2019) presents a 3D MIKE numerical model of the hypersaline Urmia lake in Iran to face water mismanagement in the basin successfully capturing the salinity distribution over the model domain; in the same area, Sedighkia and Datta (2024) have developed a TUFLOW 2D hydrodynamic model of one of the important dams in the Tehran province was developed and calibrated for simulating salinity in the reservoir and a reliable method to integrate environmental requirements of dams' lake with the reservoir operation was proposed as a new method of environmental reservoir operation; furthermore, an application of the EFDC model to estimate the extent of seawater intrusion for the total reach of the Seomjin River basin can be found in Ahn et al. (2020) where the results showed a salt water intrusion up to 16.52 km along the river reach. However, single surface models simplify groundwater behavior, and, in the same way, groundwater models consider surface waters in a simple way (Wang and Chen, 2021).

That's why to discern between different processes that can trigger and/or exacerbate groundwater salinization, considering and modeling both surface and groundwater systems is pivotal but presents many challenges. Limited data availability and human and computational resources are often restricting the possibility of developing proper models able to describe these complex environments (Ntona et al., 2022). Moreover, these challenges are heightened when studying tangled 3D geological environments, where topography and aquifer parameters can vary substantially over short distances (Turgeon et al., 2018).

Despite the need of considering both surface and subsurface water bodies to gain a proper understanding of salinization dynamics in low-lying deltaic areas, few studies in the literature have integrated groundwater and surface transport simulations and application of fully and semi-coupled models are not yet routine (Turgeon et al., 2018). This is also testified by recent review papers on surface–groundwater interactions (Ntona et al., 2022; Haque et al., 2021). In the last decades, the USGS and the US Army Corps of Engineers are combining resources to merge the capabilities of MODFLOW and HEC-RAS to address the need for a more detailed surface–subsurface modeling approach via OpenMI (Open Model Interface). This interaction is designed at the time step level so that the programs can share data and compute results on an iterative level (Fenske et al., 2011). Some research tried to design a new coupling mathematical model scheme, like Rodriguez et al. (2008) that iteratively coupled HEC-RAS and MODFLOW to improve the representation of hydraulic profiles in drain channels within a regional groundwater flow system, not focusing on salinity nor transport simulations. Others experimented different coupling approaches and numerical codes to study solute transport processes. For instance, Yuan et al. (2011) studied the interaction between surface water and groundwater flow and solute transport processes in coastal lagoons, using ELCIRC to simulate water flow and solute transport in surface bodies and SUTRA for simulating variably saturated variable-density fluid flow and solute transport in porous media. Yang et al. (2013) estimated the effects of tides and storm surges on coastal aquifer salinization via coupled surface–subsurface modelling. Zhang et al. (2023) conducted a series of numerical simulations to quantify the influence of tidal dynamics of rivers on SWI in coastal aquifers, employing a transient variable-density flow SEAWAT and SFR2-based coupled model to quantify interactions between surface water and groundwater.

This interesting research, together with others in literature, has developed fascinating and complex modeling approaches mainly focusing on the intricate interplay between surface and subsurface systems in response to tidal intrusions, without considering other salinization mechanisms such as trapped paleo-seawater. In this framework, the present study aims to fill this gap quantifying aquifer salinization dynamics in the Volturno River (VR) coastal aquifer in Campania Region (Italy) via solute transport numerical modelling and distinguishing among different salinization mechanisms separately: (i) actual seawater wedge from the coast, (ii) seawater encroachment within the VR riverbed, and (iii) paleo salinity. The VR coastal aquifer is of particular interest, since it's located in the middle of the Mediterranean region, a hot-spot of the ongoing CC (Lionello and Scarascia, 2018), and could be considered representative of many other coastal porous aquifers stressed by CC. Recent findings on this area have already highlighted (i) a clear SWI throughout the VR during low river discharge periods (Gaiolini et al., 2023), and (ii) the presence of hypersaline layers scattered a few kilometres (up to 15 km) from the coastline (Ruberti et al., 2022; Schiavo et al., 2023; Tarallo et al., 2023; Colombani et al., 2024), providing valuable results to support the simulations and thereby deepening the understanding of this coastal aquifer and its connections with the VR. A semi-coupled modelling approach was adopted to investigate the relationship between the groundwater systems and the river over a decade (2010–2020). The information gained by the transient model over the period 2010–2020, is particularly interesting given that in the VR area the relative change of mean atmospheric temperature rose from +0.97 °C in 2010 to +1.42 °C in 2020 respect to the baseline period 1850–1900 (Copernicus CIMP6 CS3, 2024). HEC-RAS water quality module and SEAWAT model were run and calibrated independently as single models and data were exchanged in a one-way interaction (HEC-RAS → EAWAT). As far as the authors are aware, no other studies in the literature have integrated HEC-RAS water quality simulations within a SEAWAT 3D transport model to quantify salinization dynamics in a coastal aquifer over a decade period. Moreover, the differentiation among salinization mechanisms, coming from a rigorous modelling approach, was not explored before and the developed methodology could be replicated in other coastal areas that are facing salinization problems like the VR area.

2. Study area

The Campania Plain (Southern Italy) is characterized by diverse economic and ecological services, hosting numerous agricultural activities, tourist facilities, and valuable protected wetlands. The entire plain is located within a vast sedimentary basin that formed during the Quaternary and still undergoes active subsidence (Matano et al., 2018). Its current geomorphological peculiarities are the result of late Holocene sedimentary evolution together with anthropic interventions, such as the expansion of urban settlements, land reclamation works, and intensive agriculture (Matano et al., 2018; Busico et al., 2021).

The modelled area is the terminal part of the floodplain at the mouth of the VR, comprising the last 13 km of the river reach. Longitudinally the study area is bounded by the Agnena river to the North and the Regi Lagni drainage channel to the South. This low-lying area presents an average altitude between −2.0 and −4.0 m a.s.l., it has a perimeter of 38.7 km and an area of approximately 91 km^2 (Fig. 1).

Originating at an elevation of approximately 1,300 m, the VR starts flowing from the province of Isernia, in Molise (Italy), passing through several geological formations before reaching the Tyrrhenian Sea.

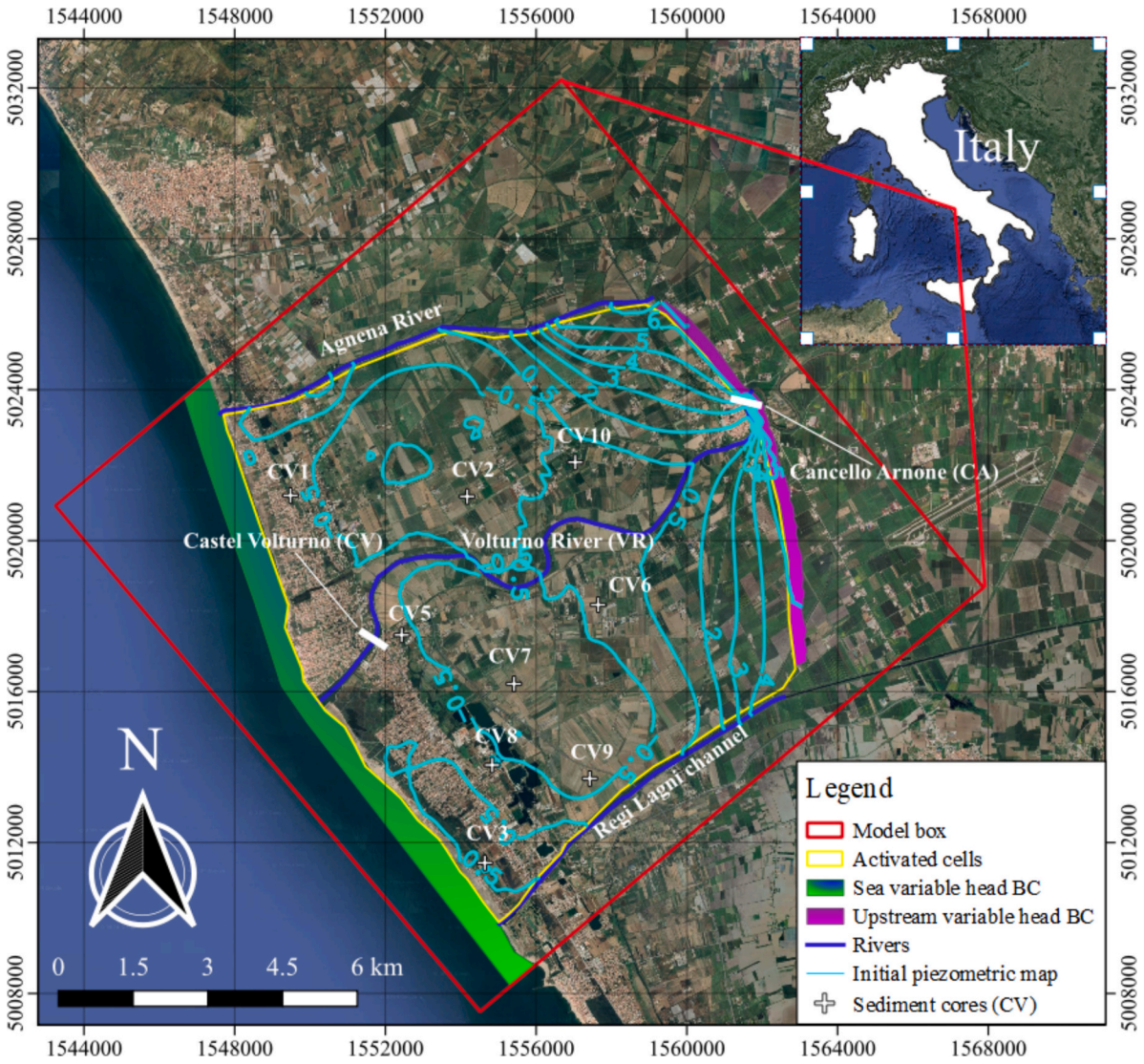

Fig. 1. Map of the study area illustrating model area and boundaries together with rivers, initial piezometry, and sediment cores used for validating the model.

Tectonic activity, volcanism, and eustatic variations have shaped the final reach of the VR over a long period of time (Corrado et al., 2018; Ruberti et al., 2022). The unconfined coastal aquifer is embedded in actual and ancient sandy deposits of dunes, crossed by fluvial paleo-channels interlayered with silty and peaty lenses (Amorosi et al., 2012; Corrado et al., 2020). A pro-deltaic unit, formed by silty clay sediments, served as the local aquiclude for the coastal aquifer. This area coincides with the point of maximum transgression during the last Holocene deglaciation, dating back to 6.5 Ky B.P. (Matano et al., 2018), with a lagoonal environment that lasted until 3.0–3.5 Ky B.P. (Corrado et al., 2020; Ruberti et al., 2022).

3. Materials and methods

To quantify the areal extent and timing of salinization within the VR coastal plain and discern amongst different processes (i.e., river-aquifer exchange, actual versus paleo SWI), a semi-coupled numerical modelling approach was employed. A 1D HEC-RAS numerical model was built up and run for a decade (2010–2020) to determine the salinity concentration distribution along the river reach. The results were used as input of a complex density-dependent 3D SEAWAT model that incorporated salinity variations on a monthly basis for the same period, to further evaluate the salinization of the aquifer. HEC-RAS water quality model and SEAWAT were run and calibrated independently, data were exchanged sequentially in a one-way interaction, using the HEC-RAS model outputs as input river boundary conditions (i.e., river water levels and concentrations) for the 3D SEAWAT model.

3.1. HEC-RAS setup

The same river geometry of Gaiolini et al. (2023) was used to build up the HEC-RAS model. A digital elevation model (DEM) with spatial resolution 2 x 2 m was used to extract the topographical data of the VR flood plain (Busico et al., 2021). Actual cross-sections were provided by the local basin authority and processed in GIS environment. Heights of the river levees were determined by the DEM and Google Earth view. Bridges were incorporated into the model, with uncertainty on the size of the bridge deck and the quantity and size of piers in the Google Earth perspective.

Hydrometric levels at the river gauges located at Cancello Arnone (CA) and Castel Volturno (CV) were retrieved from the Centro Funzionale Multirischi (CFM, 2023) of the Campania Region Civil Protection Agency website, spanning from 1st January 2010 to 31st December 2020. Daily data were subsequently monthly averaged according to the temporal resolution used in the SEAWAT simulation. Time series of Tyrrhenian Sea level data were downloaded from Copernicus Marine

Service (CMEMS, 2023) from 1st January 2010 to 31st December. The MATLAB environment was used to read the Copernicus data (Ferris, 2020), then transformed into monthly averages. Stage hydrograph boundary conditions were assigned to the most upstream (CA river gauge) and the most downstream (mouth of VR) cross-sections (Fig. 1).

A 1D unsteady flow simulation was performed to study the hydrodynamic regime that is affecting the estuarine salinity distribution (Yoon and Woo, 2015). The simulation plan was designed to run the model over the whole hydrologic decade (2010–2020), choosing a monthly output temporal resolution based on the SEAWAT model boundary conditions. Since the focus is on long-term aquifer salinization dynamics driven by riverbed leakage, the influence of tides (operating on much shorter timescales) was not considered in the modelling approach, as these short-term fluctuations were masked by the broader monthly sea level and river discharge variations.

The hydraulic model calibration was based on the comparison between simulated and measured water elevation at CV river gauge for the year 2014 (from CFM repository, Table 1), retrieving good model performance indicators (Gaiolini et al., 2023).

To model the evolution of salinity along the river reach, the HEC-RAS Water Quality module was used, based on the one-dimensional advection–dispersion equation, which allows to model the fate and transport of constituents of different kind, e.g. water temperature, dissolved oxygen, salt (Brunner, 2010):

$$\frac{\partial(AC)}{\partial t}+\frac{\partial}{\partial x}(VAC)=\frac{\partial}{\partial x}\left[D_x A\frac{\partial C}{\partial x}\right] \quad (1)$$

where C is the salinity concentration [ML^{-3}]; D_x is the longitudinal dispersion coefficient [L^2T^{-1}]; V is the flow velocity [L^3]; A is the cross-sectional area [L^2]. D_x together with the boundary condition values of salinity concentrations must be entered by the user for the salinity concentration to be simulated as a single parameter.

A freshwater salinity concentration value of 0.4 g/L, based on the analysis of the historical major ions concentrations at the Capua measuring station (ARPAC, 2023), was assigned to the upstream boundary at CA river gauge and a seawater salinity value of 38 g/L was assigned to the downstream boundary at the VR mouth (Sorgente et al., 2020). D_x was calculated using the same approach of Gaiolini et al. (2023), i.e. applying Fischer's equation and allowing for a longitudinal

Table 1
National and worldwide databases used to constrain the model.

Dataset	Parameter	Repository	URL
Soil	Grain size distribution	ISRIC	https://maps.isric.org
Geology	Aquifer thickness	ISPRA	https://sgi2.isprambiente.it/viewersgi2
Hydrogeology	Hydraulic conductivity	ISPRA	https://sgi2.isprambiente.it/viewersgi2
CORINE Land Cover	Land Use	COPERNICUS	https://land.copernicus.eu/pan-european/corine-land-cover
SEALEVELEURP HYL4MY008068	Sea levels	CMEMS	https://doi.org/10.48670/moi-00141
Hydrometric station	Rivers stages	CFM	https://centrofunzionale.regione.campania.it/#/pages/sensori/sensor-utility
BIGBANG40	Evapotranspiration	ISPRA	https://www.isprambiente.gov.it/pre_meteo/idro/BIGBANG_ISPRA.html
BIGBANG40	Recharge	ISPRA	https://www.isprambiente.gov.it/pre_meteo/idro/BIGBANG_ISPRA.html

spatial distribution of the coefficient based on the calculation of the hydrodynamic parameter at each cross-section (Brunner, 2010). Based on the unsteady flow simulation, the simulation plan was scheduled to run for the whole hydrologic decade (2010–2020).

3.2. SEAWAT set-up

The transport simulations were performed by means of SEAWAT to mimic the interconnections between the sea, the groundwater, and the VR. The model was downscaled from a large MODFLOW model of the whole Campania Region, that was already calibrated against an observed piezometric map of the Campania region for the year 2000 and validated by exploiting a secondary elaboration of the global groundwater depth dataset for the year 2013 (Gaiolini et al., 2022).

SEAWAT simulates variable-density groundwater flow and transport using the same finite-difference method to solve the groundwater flow equation (Guo & Langevin, 2002):

$$\nabla^*\left[\rho\frac{\mu_0}{\mu}K_0\left(\nabla h_0+\nabla z\frac{\rho-\rho_0}{\rho_0}\right)\right]=\rho S_{s,0}\frac{\partial h_0}{\partial t}+\theta\frac{\partial\rho}{\partial C}\frac{\partial C}{\partial t}-\rho_s q_s' \quad (2)$$

where ρ is the fluid density [ML^{-3}]; ρ_0 is the fluid density at the reference concentration and reference temperature [ML^{-3}]; μ is the dynamic viscosity [$ML^{-1}\ T^{-1}$]; μ_0 is the dynamic viscosity at the reference concentration and reference temperature [$ML^{-1}\ T^{-1}$]; K_0 is the hydraulic conductivity tensor of material saturated with the reference fluid [-]; h_0 is the hydraulic head measured in terms of the reference fluid of a specific concentration and temperature [L]; z is the upward coordinate direction aligned with gravity; t is time [T]; $S_{s,0}$ is the specific storage [L^{-1}]; θ is the porosity [-]; C is the salt concentration [ML^{-3}]; q_s' is a source or sink of fluid with density ρ_s [T^{-1}].

A fully transient simulation, based on a time discretization of 132 stress periods of 1-month each, was performed to represent the change in salinity during the simulation time (2010–2020).

The model consisted of 90 rows, 90 columns, and 7 layers with variable thickness. The first layer was thicker than the others, with the purpose of containing the water table variations and avoid dry cells that lead to convergence problem (Brunner et al., 2010). In this way, grid cells wetting and rewetting was avoided, thus eliminating the numerical oscillations and solver nonconvergence connected with this process. The rows and columns had square sizes of 147 x 147 m. Initially, all the hydrogeological parameters used in the calibrated and validated MODFLOW model (Gaiolini et al., 2022) were kept unchanged. The horizontal hydraulic conductivity values range from $1x10^{-6}$ m/s in the coastal part of the VR coastal aquifer, where clay layers are present, to $3.3x10^{-4}$ m/s where more permeable alluvial deposits exist. The model domain was divided into polygons whose extensions correspond to the extension of the different geological formations of the Campania region (Fig. 2).

To account for internal layering, the vertical hydraulic conductivity was set at one tenth of the horizontal hydraulic conductivity, while the effective porosity was kept as 0.2 for the entire model to keep the model as simple as possible given the lack of specific and reliable data. The specific storage (S_s) was set to $1x10^{-4}\ m^{-1}$ as function of the compressibility of the water and the elastic property of the soil matrix. A specific yield (S_y) of 0.2 was used as function of porosity (Bear and Braester, 1972). The diffusion coefficient was assumed to be equivalent to $1x10^{-9}\ m^2/s$ and a longitudinal dispersivity value of 2 m was used for the entire domain to optimize the calibration procedure.

Both evapotranspiration and recharge rate data were retrieved using the BIGBANG 7.0 hydrological balance developed by ISPRA (Braca et al., 2019). QGIS 3.36 software (https://www.qgis.org) was used to process the data by trimming the files based on the model area, change coordinates and format to simulate them within the Evapotranspiration and Recharge Package (EVT and RCH), respectively. The maximum transpirable salinity was set to 15 g/L for the entire model due to the

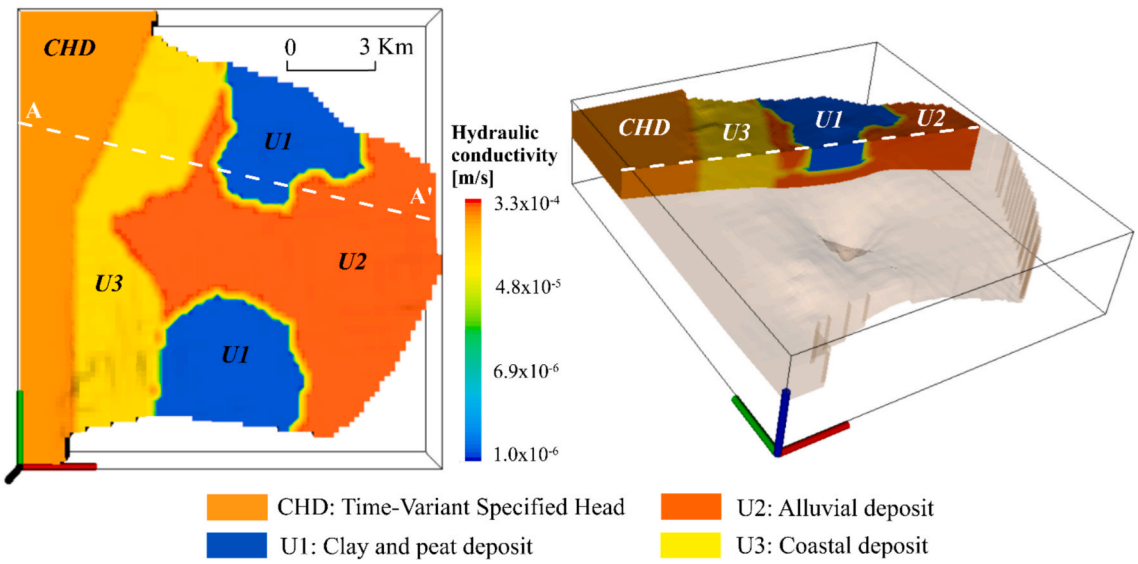

Fig. 2. Plan (left panel) and 3D cropped views along AA` section (right panel) of the model domain, showing the spatial distribution of the hydraulic conductivity values used to represent the different geological formations.

presence of halophytic vegetation (Mastrocicco et al., 2019).

The river heads and salinities were obtained from the HEC-RAS flow and transport simulations and imported via polyline input method within the River Package (RIV).

The same CMEMS dataset was used for the Tyrrhenian Sea level oscillation and imported as boundary condition within the Time-Variant Specified Head Package (CHD). Groundwater levels along the closure transect were obtained from the regional-scale model (Gaiolini et al., 2022) and imported as upstream boundary conditions within the same Package.

All national and worldwide databases about aquifer properties and boundary conditions used to inform the model are depicted in Table 1.

At the beginning of a transport simulation, SEAWAT requires the initial concentration of each active species at each active cell. The same values of 0.4 g/L and 38 g/L were used accounting for a freshwater salinity concentration and a seawater salinity value, respectively.

In a first step, only sea and river salinity concentrations retrieved from HEC-RAS were imported as initial conditions. This approach aimed to exclusively quantify the impact of actual SWI directly from the sea or via preferential surface bodies, i.e. the VR, which subsequently exchanges water with the aquifer leading to its salinization. Initially a steady state simulation was performed for 100 years considering averaged boundary conditions to reach the full development of the seawater wedge along the coast and the salt intrusion within the VR final reach. Then, the final heads and concentrations calculated by SEAWAT were imported as initial conditions in the transient model with variable boundary conditions. By employing this method, it was possible to assess the dynamics of exchange between marine and riverine systems with the aquifer, elucidating the relative contribution of each source to the groundwater salinization processes.

Finally, to allow a more realistic representation of the salinization patterns within the study area, the 2D stochastic ensemble mean saline concentrations calculated by Schiavo et al. (2023) were used as initial concentration. Again, a steady state simulation considering average boundary conditions was performed for 100 years to distribute these concentrations across the model domain before applying variable boundary conditions in the transient model. This comprehensive approach incorporated the complexities of spatial variability in salinity, including the influence of paleo SWI, and enabled the simulation of long-term salinity dynamics within the aquifer system. The groundwater flow model was already calibrated and validated (Gaiolini et al., 2022), as well as the HEC-RAS model (Gaiolini et al., 2023), and thus both were kept unchanged. Nine sediment cores (Fig. 1), perforated down to a depth of 30 m (b.g.l.) and drilled with a continuous coring system, were used to capture vertical salinity distribution within the study area (Colombani et al., 2024) and calibrate the transport model. The SEAWAT model was calibrated via trial-and-error technique, manually adjusting locally the initial concentrations and varying the effective porosity and dispersion values to match the observed salinity profiles in the sediment cores (Fig. 1). The procedure was performed considering both the developed 2D groundwater salinity map and the calculated salinity distribution within the river, cross validating the river transport simulation. In the field, the position of each sediment core was selected to capture the local vertical variability of the subsoil, sampling the cores in the presence of variations in grain size, color, or incidence of fragments. To obtain the vertical distribution of salinity, the sediments were analysed using a 5TE Decagon TDR, which measures the volumetric water content, temperature, and bulk electrical conductivity (EC) of the sediments. Bulk EC was converted to porewater EC using the Hilhorst (2000) relationship and then into salinity concentration.

4. Results and discussions

4.1. Validation of the transport model

The model accurately captures the salinity distribution in the aquifer, despite some limitations in representing vertical heterogeneities. The validation process has ensured accuracy in the representation of the complex spatial and temporal patterns of salinity within the study area, thus providing a reliable tool to quantify and discern amongst different salinization processes.

Fig. 3 shows the validation results of calculated versus measured salinity values, together with a comparison between vertical profiles in all the sediment cores. Model performance indicators (R^2, NSE, and RMSE) were computed indicating that a relatively good model validation was achieved for salinities throughout the aquifer showing the presence of brackish to saline groundwater. Moreover, SEAWAT results were capable to mimic quite effectively the vertical distribution of salinity within the domain. Nonetheless, in some of the layers the model failed to reproduce the measured salinity values and these points are depicted in red (Fig. 3a). Panels a and b show how model performance indicators change considering or not these points in the simulation, underscoring the challenge of simulating local scale vertical heterogeneities in a large-scale model, where small lenses affecting local

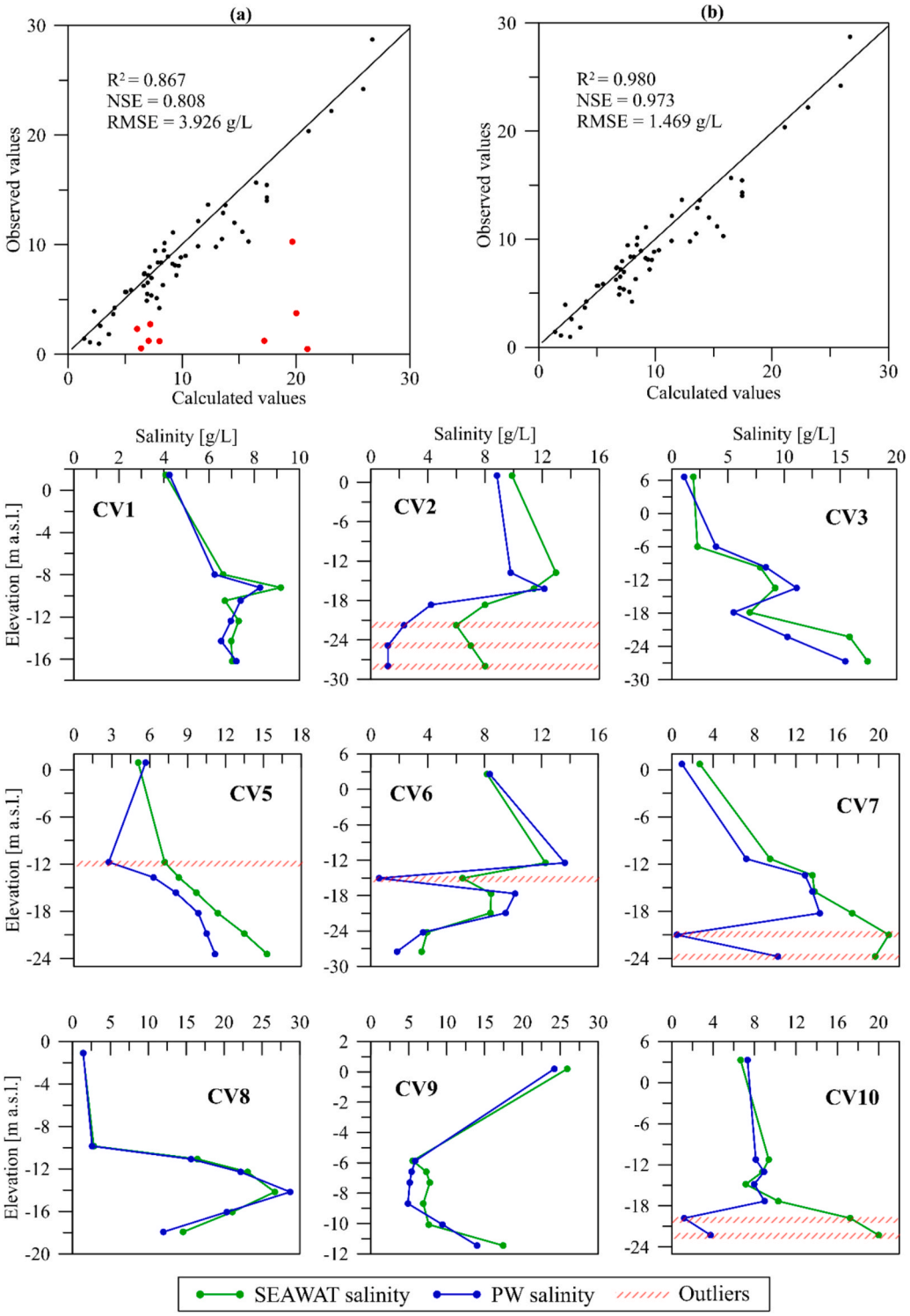

Fig. 3. Concentration scatter diagrams with (a) and without outliers (b). In the lower panels the comparison between SEAWAT and porewater salinity profiles is represented for all the sediment cores. The scattered red bands underline the depth of each outlier. (For interpretation of the references to color in this figure legend, the reader is referred to the web version of this article.)

groundwater flow and solutes transport are not included. The outliers were also highlighted in lower panels of Fig. 3 (scattered red bands) indicating that the model tends to overestimate the salinity in those spots, while the measured values are usually very low. This discrepancy arises from the presence of sandy deposits within the cores that were rapidly flushed by meteoric recharge because of their higher hydraulic conductivity (Ruberti et al., 2022). Unfortunately, modelling this kind of vertical heterogeneities results to be really complex not knowing salinity desorption rates of the subsoil, e.g. in presence of clay and peat lenses characterized by high ions exchange capacity.

4.2. *Model based SWI assessment*

The HEC-RAS transport model provided an estimate of the salinity

distribution along the VR, highlighting seasonal variations and long-term trends. Fig. 4 shows that concentration values in each considered cross-section throughout the VR oscillate during the simulation according to seasonal changes in the river discharge: high river salinities correspond to low river discharge periods (summers), while low salinity values are observed during high river discharge periods (winters). The salinity in the final reach of the VR is gradually ascending from 2010 to 2020 (red and green lines). Specifically, at the mouth of the river (red lines in Fig. 4), salinity linear trend increases from nearly 20 to over 30 g/L. This behaviour can be attributed to progressively decreasing discharges of the VR (black lines in Fig. 4), where the linear trend drops from a value of almost 25 m^3/s to just few cubic meters per seconds above the zero over the decade. Considering a monthly temporal resolution for the simulation, tidal forcing, that resulted to be very influential in changing the river salinity distribution during low discharge periods (Gaiolini et al., 2023), is masked by seasonal changes in sea level and river discharge.

Even if the 1D modelling approach inherently simplifies the representation of the complex interactions involved at the estuary, the simulation provided a useful understanding of the river salinization mechanisms over a decade. Quantifying the salinity distribution along the VR was pivotal in absence of salinity measurement campaigns, granting to feed the SEAWAT model to further investigate aquifer salinization and have an idea of the salt mass exchange amongst surface- and groundwater.

Building on the insights gained from the HEC-RAS model, the 3D SEAWAT model allowed to produce salinity maps and trends (Figs. 5 and 6) that provided valuable understanding of the aquifer salinization processes, thus enabling to understand the role and magnitude of different mechanisms at play. Fig. 5 shows the comparison between model generated salinity maps at the end of the simulation, considering actual SWI (left panel) and paleo SWI (right panel) separately.

Considering just the actual SWI (left panel), spikes of salt mass within the aquifer were triggered by the lowering of the VR discharge during several summer seasons, resulting in an S-shaped salinity distribution following the river's meander (left panel in Fig. 5). The classical mechanism of seawater wedge intrusion from the coastline was minimal compared to the salinization from the VR bed leaching. Evidently, the area occupied by high salinity concentrations within the aquifer is wider including paleo SWI within the model (right panel). Some zones exhibit highly saline groundwater with concentration values up to 75 g/L, nearly doubling the actual Tyrrhenian Sea salinity. This is due to remnant paleo seawater trapped into peaty and silty-clay sediments that further complicated the groundwater salinity distribution, as already recently recognized (Schiavo et al., 2023).

Lower panels of Fig. 5 show two cross-sections passing through the final reach of the VR (AA') and through the point of maximum actual seawater wedge (BB'). High salinity areas tend to drift to the bottom of the aquifer due to meteoric recharge that is freshening the uppermost part. In section BB', it is evident that the propagation of the seawater wedge along the coastline during the period of study is minimal and observed to be less than 150 m. This is most probably due to the high submarine groundwater discharge along the whole Campania coastline as estimated by Gaiolini et al. (2022). Since freshwater is less dense than seawater, the actual seawater creates a wedge in the lower part of the aquifer (Bakhtyar et al., 2012) resulting in higher concentration values at deeper layers of the aquifer along the coastline (see CV1 and CV3 salinity profiles in Fig. 3).

Actual aquifer salinization is driven primarily by seawater ingression through the VR that behaves as a preferential pathway to intrusion during low discharge periods (Cui et al., 2015; Setiawan et al., 2023).

The model including the paleo SWI simulates higher salinity values in each sediment core, but CV5 located near the final part of the VR reach (Fig. 6). In this area the actual SWI through the river is prevailing on the paleo SWI. The concentration values, as well as the increasing/decreasing behavior in all the analyzed trends throughout the simulation depend on each sediment core position related to the morphology of the area and to recharge/evapotranspiration patterns distribution within the model domain.

To further quantify SWI, a mass/concentration balance was performed considering both actual and paleo SWI (Fig. 7). Such a balance allowed for the estimate of the total amount of salt mass and concentration accumulated within the aquifer over the simulation. The model including the paleo salinity revealed salinity values nearly an order of

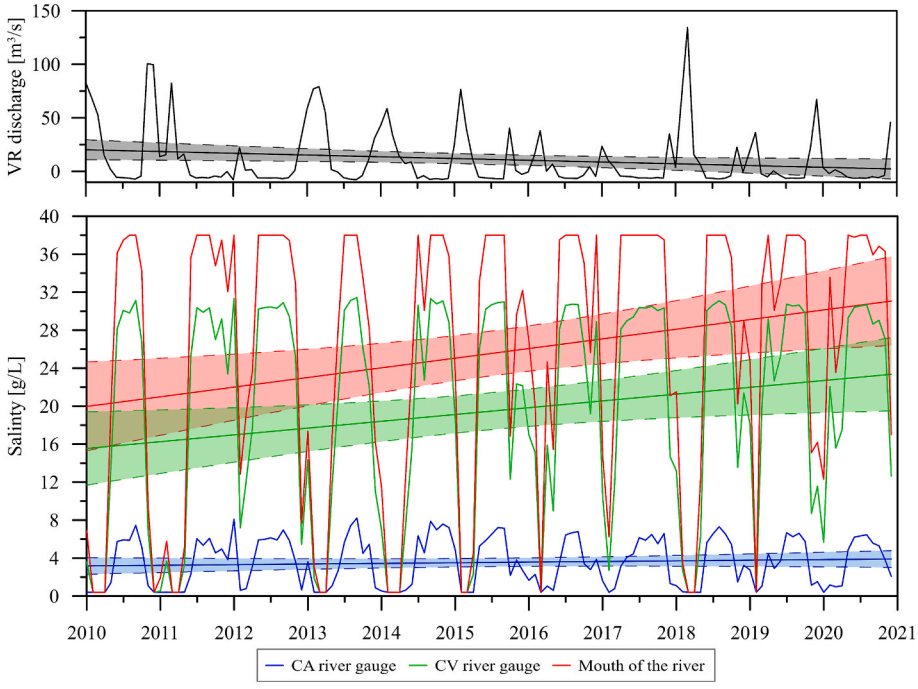

Fig. 4. VR discharge calculated at CA river gauge (upper panel) and salinity oscillation within the main cross-sections during the simulation time (lower panel). Salinity and discharge linear trends (solid lines) with related 95% confidence intervals (shaded areas bounded by dashed lines) are also reported.

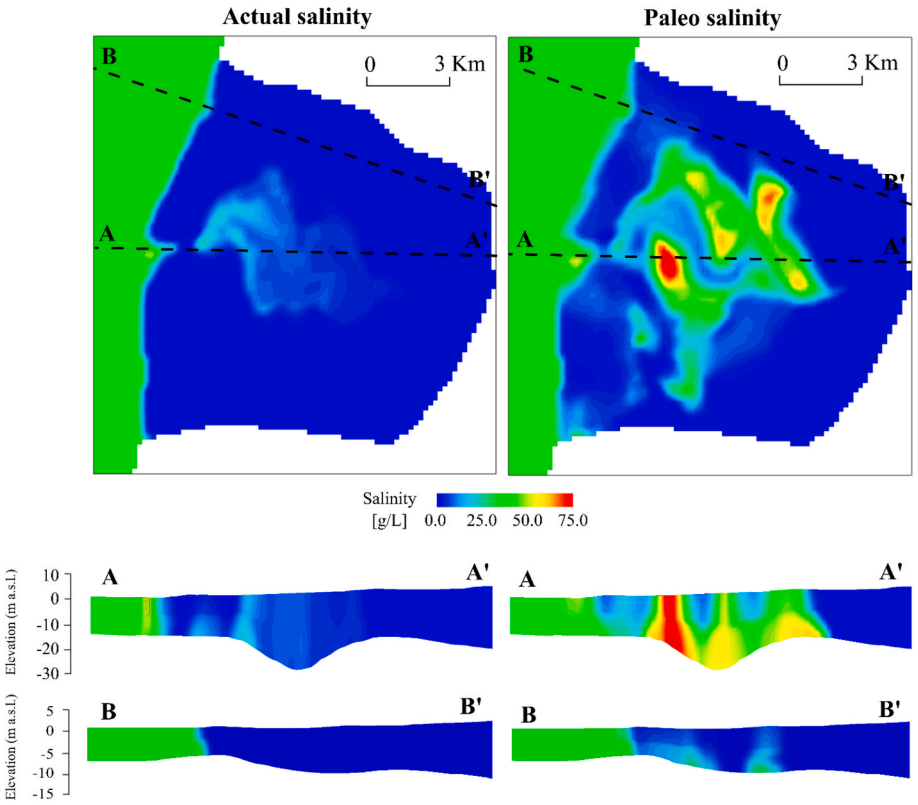

Fig. 5. Calculated salinity concentration maps (upper panels) together with two selected cross sections (lower panels) considering both actual (left panels) and paleo seawater (right panels) intrusion mechanisms. The end of simulation was used as selected time for the snapshot.

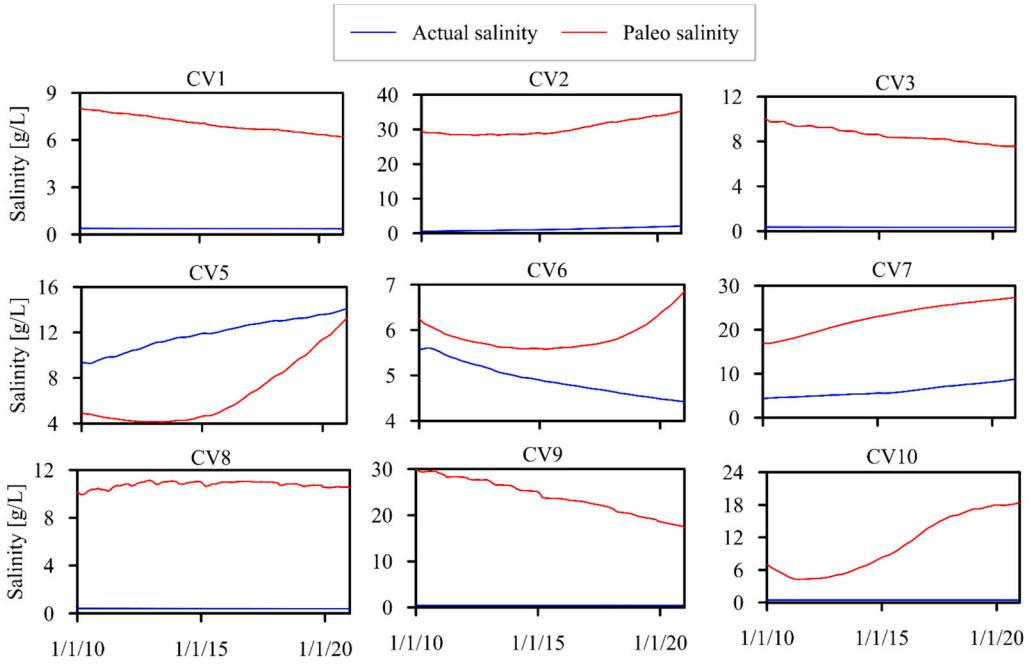

Fig. 6. Calculated salinity trends for all the observation points: comparison between actual (blue lines) and paleo SWI (red lines). (For interpretation of the references to color in this figure legend, the reader is referred to the web version of this article.)

magnitude higher than the model considering just the actual SWI. Specifically, the total mass amount of salinity accumulated within the aquifer due to actual SWI at the end of the simulation is 5.69 x 10^3 tons, whereas paleo salinization contributed 1.14 x 10^4 tons (Fig. 7), thus doubling the mass of salt in the aquifer. The actual scenario is showing increasing trends of both mass and concentration because of rising river salinity due to a reduced river discharge according to HEC-RAS simulation. In contrast, the one including paleo salinity exhibited a decreasing trend in both mass and concentration because of the freshening due to the regional discharge from the karst massifs (Gaiolini

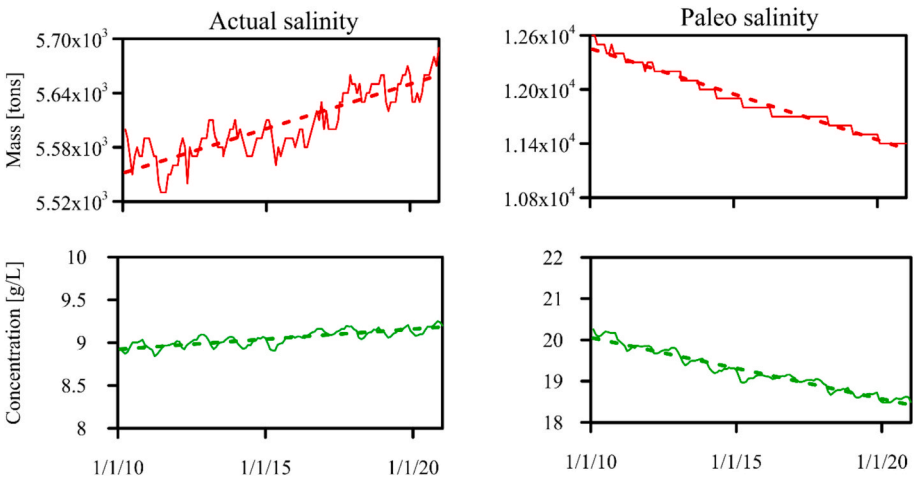

Fig. 7. Calculated trends of total salinity mass (red lines) and concentration (green lines) accumulated within the aquifer system over the simulation: comparison between actual (left panels) and paleo SWI (right panels). (For interpretation of the references to color in this figure legend, the reader is referred to the web version of this article.)

et al., 2022) that flushes salty peaty-clayey sediments within the aquifer. This outcome is consistent with the freshening trend estimated via Base Exchange index values by Colombani et al. (2024) in the same area, further suggesting that high salinities are attributable to evapoconcentrated paleo-seawater entrapped within sediments then flushed by recharge waters from rain and rivers (Meyer et al., 2019).

Recognizing paleo SWI as the main cause of coastal aquifer salinization prevents managers and companies from useless interventions and actions to avoid the actual intrusion of the seawater wedge from the coast that are often expensive and time-consuming.

4.3. Water budget calculation under hydrological variability

Reduced meteoric recharge and decreasing river discharges are altering groundwater dynamics, thereby affecting aquifer salinization processes. Fig. 8 shows calculated heads in each of the sediment cores used as observation points to assess the water table variability over the simulation time. Piezometric heads oscillate seasonally according to recharge and evapotranspiration patterns presenting peaks and troughs during wet and dry season, respectively. A clear declining trend of the piezometric heads was observed at each observation point (dashed blue lines in Fig. 8). To better explain the lowering of the water table over the 10 years of simulation, Processing Modflow ZoneBudget routine (Harbaugh, 2005) was run and the volumetric water budget within the model domain assessed, accounting for recharge, evapotranspiration, and river-aquifer water volume exchange (Fig. 9).

Recharge and evapotranspiration represent the major inflow and outflow to/from the aquifer system. Both vary throughout the simulation depending on seasonal changes in precipitation and temperature. High recharge values are observed during wet seasons, reaching maximum flow rate of almost 2 m^3/s, while evapotranspiration values reach their maximum flow rate of almost 1.5 m^3/s during dry seasons, when temperatures are higher. Recharge presents a declining trend over the simulation time acting as the main constrain to groundwater

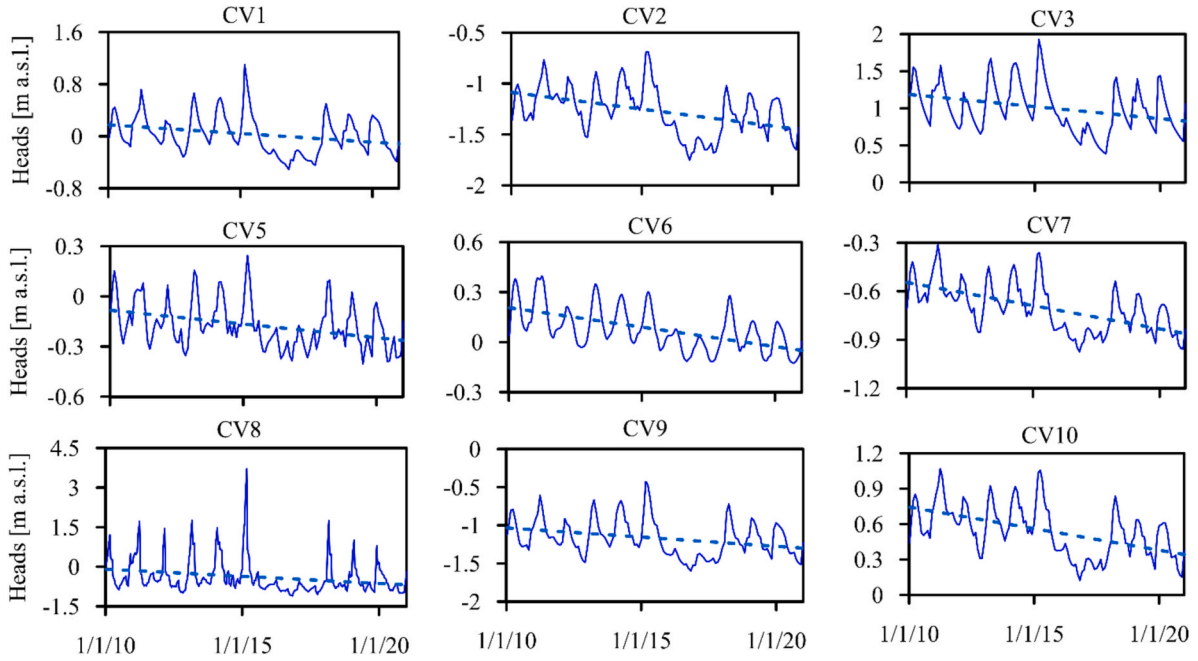

Fig. 8. Calculated piezometric heads (solid blue lines) and relative linear trends (dashed blues lines) over the simulation period for all the observation points. (For interpretation of the references to color in this figure legend, the reader is referred to the web version of this article.)

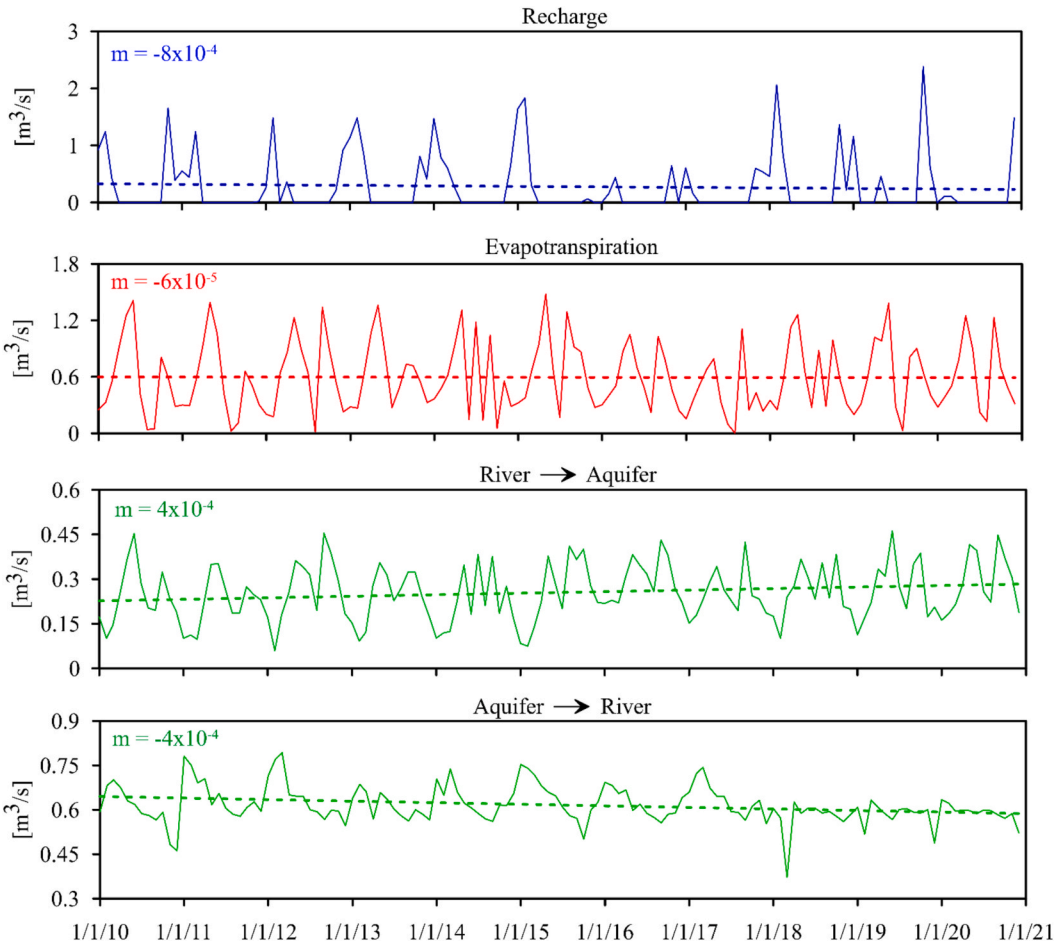

Fig. 9. Calculated water budget: recharge (blue line) and evapotranspiration (red line) were shown as maximum water inflow and outflow to/from the aquifer, respectively, together with river-aquifer water exchange (green lines). Linear trends (dashed lines) and relative angular coefficients (m) were depicted for each water budget component. (For interpretation of the references to color in this figure legend, the reader is referred to the web version of this article.)

availability and leading to the observed lowering of the calculated piezometric heads. Despite a general increase in mean atmospheric temperatures (from 16.4 °C in 2010 to 16.9 °C in 2020), evapotranspiration is slowly declining with a quite steady linear trend (the angular coefficient m of the evapotranspiration trend is an order of magnitude less than the one describing the recharge trend) over the simulation time. This behaviour is most probably due to the lowering of the water table which is reducing the amount of water available for direct evaporation by exceeding the evapotranspiration extinction depth (Colombani et al., 2021). River-aquifer water exchange is also represented in Fig. 9, varying significantly across the seasons. The flow rate at which the aquifer is feeding the river (ranging from 0.37 to 0.79 m^3/s) is higher than the river contribution to the aquifer (ranging from 0.06 to 0.46 m^3/s). However, the flow from the aquifer to the river is observed to decline over the simulation, while the water flowing from the river to the aquifer is on the ascendancy. The depletion of groundwater resources due to reduced meteoric recharge is shifting the equilibrium of the river-aquifer system, leading to an increase in water flowing from the river to the aquifer. Since VR was identified as a preferential pathway for actual SWI, this phenomenon could alter the salinization dynamics, worsening the groundwater quality when the river waters are mainly saline or brackish.

While this study provides valuable insights on river-aquifer interactions, it is crucial to acknowledge limitations and uncertainties when interpreting the results. The simulation effectively captures the seasonal river-aquifer flow exchanges shown in Fig. 9, as the groundwater response is relatively slower compared to the river dynamics and the river monthly fluctuations were integrated as time-dependent boundary conditions within the model. However, the use of a one-way and independent model running procedure intrinsically simplifies the representation of these complex interactions involved and may lead to some level of loss in capturing the real time feedback from the aquifer to the river. Different coupling methods are subject to different errors and, since different error patterns are also associated with the numerical schemes used to solve the surface and subsurface components, it is extremely complicated to attribute error to the coupling method (Furman, 2008).

5. Conclusions

The semi-coupled modelling approach used in this article allowed to discern amongst different sources of aquifer salinization that are commonly not well differentiated. The VR coastal area here selected to implement the modelling approach is of particular interest to quantify the ongoing CC effects on coastal groundwater resources, given its location in the middle of the Mediterranean Region a hot-spot of CC. The implemented transient numerical model provided a comprehensive identification of the salinization mechanisms, enabling for an accurate groundwater and mass balance calculation. In the absence of monitoring campaigns along the VR, the HEC-RAS simulation estimated river salinity distribution that was crucial to assess the contribution of surface bodies to aquifer salinization dynamics. The SEAWAT model captured the salinity vertical distribution over the model domain quite reliably except for some small sandy lenses, where it tended to overestimate the

measured values. Key findings indicate that: (i) actual SWI was prevailing along the final reach of the VR, which acted as a preferential pathway for SWI due to reduced river discharge; (ii) paleo SWI resulted to be the major driver of the presence of highly saline groundwater within the aquifer, while the seawater wedge was limited to a maximum of 150 m inland. These patterns could be considered the rule rather than the exception in similar low-lying deltaic systems.

The model also captured seasonal variations in piezometric heads, highlighting a gradual decline due to reduced recharge rate imputable to the ongoing CC, which consequently alter the river-aquifer interactions and salinity dynamics. The major limitations of this semi-coupled modelling approach are the (i) impossibility to have feedback from groundwater into the river system and (ii) the simplified vertical reconstruction of the aquifer properties that cannot reproduce accurately local features.

Compared to previous studies, this research delved into a more detailed differentiation of salinization sources, emphasizing the role of paleo SWI and river-aquifer interactions. Such a comprehension can prevent unnecessary and costly interventions aimed at arresting seawater wedges from the coast, which is often not the main cause of aquifer's salinization. As global water challenges intensify, developing such surface–groundwater modelling tools is crucial in supporting authorities to make informed decisions and minimize the impact on water quality in similar environmental settings.

CRediT authorship contribution statement

Mattia Gaiolini: Writing – original draft, Visualization, Software, Methodology, Investigation, Formal analysis, Data curation. **Abraham Ofori:** Software, Investigation, Formal analysis, Data curation. **Matteo Postacchini:** Writing – review & editing, Validation, Supervision, Conceptualization. **Micòl Mastrocicco:** Writing – review & editing, Validation, Supervision, Conceptualization. **Nicolò Colombani:** Writing – review & editing, Supervision, Methodology, Conceptualization.

Declaration of competing interest

The authors declare that they have no known competing financial interests or personal relationships that could have appeared to influence the work reported in this paper.

Acknowledgments

The authors would like to thank the European Commission and MUR for funding in the frame of the collaborative international consortium DATASET (Groundwater salinization and pollution assessment tool: a holistic approach for coastal areas, Water4All_00084), financed under the 2022 Joint call of the European Partnership 101060874 - Water4All.

Data availability

Data will be made available on request.

References

Aeschbach-Hertig, W., Gleeson, T., 2012. Regional strategies for the accelerating global problem of groundwater depletion. Nat. Geosci. 5 (12), 853–861. https://doi.org/10.1038/ngeo1617.

Alessandrino, L., Gaiolini, M., Cellone, F.A., Colombani, N., Mastrocicco, M., Cosma, Da Lio, C., Donnici, S., Tosi, L., 2023. Salinity origin in the coastal aquifer of the Southern Venice lowland. Sci. Tot. Environ. 905, 167058. https://doi.org/10.1016/j.scitotenv.2023.167058.

Amorosi, A., Pacifico, A., Rossi, V., Ruberti, D., 2012. Late Quaternary incision and deposition in an active volcanic setting: the Volturno valley fill, southern Italy. Sedim. Geol. 282, 307–320. https://doi.org/10.1016/j.sedgeo.2012.10.003.

Anderson, M.P., Woessner, W.W., Hunt, R.J., 2015. In: Applied Groundwater Modelling: Simulation of Flow and Advective Transport. Academic Press, Elsevier, London. https://doi.org/10.1016/C2009-0-21563-7.

Ahn, J.M., Lee, K., Lyu, S., 2020. Effect of changes in watershed runoff characteristics on salinity intrusion in estuary using EFDC. KSCE J. Civ. Eng. 24 (1), 87–98. https://doi.org/10.1007/s12205-020-1306-5.

ARPAC, 2023. Online database on surface water quality of Campania Region. https://dati.arpacampania.it/dataset/monitoraggio-acque-superficiali-s07 Dataset identify number: ARPA: https://dati.arpacampania.it/dataset/monitoraggio-acque-superficiali-s07. Last access on 13/03/2023.

Bakhtyar, R., Brovelli, B., Robinson, C., Li, L., 2012. Transport of variable-density solute plumes in beach aquifers in response to oceanic forcing. Adv. Water. Resour. 53, 208–224. https://doi.org/10.1016/j.advwatres.2012.11.009.

Bear, J., Braester, C., 1972. On the Flow of Two Immiscible Fluids in Fractured Porous Media. Developments in Soil Science Vol. 2, 177–202.

Bear, J., Cheng, A.H.D., 2010. Modelling Groundwater Flow and Contaminant Transport Vol. 23, 89–103.

Braca, G., Bussettini, M., Ducci, D., Lastoria, B., Mariani, S., 2019. Evaluation of national and regional groundwater resources under climate change scenarios using a GIS-based water budget procedure. Rend. Fis. Acc. Lincei 30 (1), 109–123. https://doi.org/10.1007/s12210-018-00757-6.

Brunner, G.W. 2010. HEC-RAS River Analysis System. Hydraulic Reference Manual. Version 4.1. U.S. Army Corps of Engineers, Hydrologic Engineering Centre, Davis CA.

Brunner, P., Simmons, C.T., Cook, P.G., Therrien, R., 2010. Modeling surface water-groundwater interaction with MODFLOW: some considerations. Groundwater 48 (2), 174–180. https://doi.org/10.1111/j.1745-6584.2009.00644.x.

Busico, G., Buffardi, C., Ntona, M.M., Vigliotti, M., Colombani, N., Mastrocicco, M., Ruberti, D., 2021. Actual and forecasted vulnerability assessment to seawater intrusion via GALDIT-SUSI in the Volturno river mouth (Italy). Remote Sens. 13 (18), 3632. https://doi.org/10.3390/rs13183632.

Cao, T., Han, D., Song, X., Trolle, D., 2020. Subsurface hydrological processes and groundwater residence time in a coastal alluvium aquifer: evidence from environmental tracers ($\delta^{18}O$, $\delta^{2}H$, CFCs, ^{3}H) combined with hydrochemistry. Sci. Tot. Environ. 743, 140684. https://doi.org/10.1016/j.scitotenv.2020.140684.

CFM, 2023. Centro Funzionale Multirischi of the Campania Region Civil Protection Agency. https://centrofunzionale.regione.campania.it/#/pages/sensori/archivio-idrometrici. Last access on13/03/2023.

CMEMS, 2023. Copernicus Marine Service. https://data.marine.copernicus.eu/products. Last access on 13/03/2023.

Colombani, N., Cuoco, E., Mastrocicco, M., 2017. Origin and pattern of salinization in the Holocene aquifer of the southern Po Delta (NE Italy). J. Geochem. Explor. 175, 130–137. https://doi.org/10.1016/j.gexplo.2017.01.011.

Colombani, N., Gaiolini, M., Busico, G., Postacchini, M., 2021. Quantifying the impact of evapotranspiration at the aquifer scale via groundwater modelling and MODIS data. Water 13, 950. https://doi.org/10.3390/w13070950.

Colombani, N., Alessandrino, L., Gaiolini, M., Gervasio, M.P., Ruberti, D., Mastrocicco, M., 2024. Unravelling the salinity origins in the coastal aquifer/aquitard system of the Volturno River (Italy). Water Res. 263, 122145. https://doi.org/10.1016/j.watres.2024.122145.

Copernicus Climate Change Service, Climate Data Store, (2024): Gridded dataset underpinning the Copernicus Interactive Climate Atlas. Copernicus Climate Change Service (C3S) Climate Data Store (CDS). DOI: 10.24381/cds.h35hb680 (Accessed on 13-Apr-2025).

Corrado, G., Amodio, S., Aucelli, P.P., Incontri, P., Pappone, G., Schiattarella, M., 2018. Late quaternary geology and morphoevolution of the Volturno coastal plain, southern Italy. Alp. Mediterr. Quat. 31, 23–26. https://amq.aiqua.it/index.php/amq/article/view/180.

Corrado, G., Amodio, S., Aucelli, P.P.C., Pappone, G., Schiattarella, M., 2020. The subsurface geology and landscape evolution of the Volturno coastal plain, Italy: interplay between tectonics and sea-level changes during the Quaternary. Water 12 (12), 3386. https://doi.org/10.3390/w12123386.

Cui, B., Shao, X., Zhang, Z., 2015. Assessment of flow paths and confluences for saltwater intrusion in a deltaic river network. Hydrol. Process. 29 (20), 4549–4558. https://doi.org/10.1002/hyp.10521.

Dang, X., Gao, M., Wen, Z., Hou, G., Jakada, H., Ayejoto, D., Sun, Q., 2022. Saline groundwater evolution in the Luanhe River delta (China) during the Holocene: hydrochemical, isotopic, and sedimentary evidence. Hydrol. Earth Syst. Sci. 26 (5), 1341–1356. https://doi.org/10.5194/hess-26-1341-2022.

De Louw, P.G., Essink, G.O., Stuyfzand, P.J., Van der Zee, S.E.A.T.M., 2010. Upward groundwater flow in boils as the dominant mechanism of salinization in deep polders, the Netherlands. J. Hydrol. 394 (3–4), 494–506. https://doi.org/10.1016/j.jhydrol.2010.10.009.

Dingle, E.H., Creed, M.J., Sinclair, H.D., Gautam, D., Gourmelen, N., Borthwick, A.G.L., Attal, M., 2020. Dynamic flood topographies in the Terai region of Nepal. Earth Surf. Process. Landf. 45 (13), 3092–3102. https://doi.org/10.1002/esp.4953.

Eswar, D., Karuppusamy, R., Chellamuthu, S., 2021. Drivers of soil salinity and their correlation with climate change. Curr. Opin. Env. Sust. 50, 310–318. https://doi.org/10.1016/j.cosust.2020.10.015.

Ferguson, G., Gleeson, T., 2012. Vulnerability of coastal aquifers to groundwater use and climate change. Nat. Clim. Change 2 (5), 342–345. https://doi.org/10.1038/nclimate1413.

Ferris, L., 2020. Ocean_data_tools: A MATLAB toolbox for interacting with bulk freely-available oceanographic data. J. Open Source Softw. 5 (54), 2497. https://doi.org/10.21105/joss.02497.

Furman, A., 2008. Modeling coupled surface–subsurface flow processes: a review. Vadose Zone J., 7 (2), 741–756. https://doi.org/10.2136/vzj2007.0065.

Fenske, J., Banta, E., Piper, St., Donchyts, G., Wexler, E.J. 2011. Coupling HEC-RAS and MODFLOW using OpenMI. Proceedings of the conference MODFLOW and More 2011, Golden, Denver, U.S.A.
Gaiolini, M., Colombani, N., Busico, G., Rama, F., Mastrocicco, M., 2022. Impact of boundary conditions dynamics on groundwater budget in the Campania region (Italy). Water 14 (16), 2462. https://doi.org/10.3390/w14162462.
Gaiolini, M., Colombani, N., Mastrocicco, M., Postacchini, M., 2023. Seawater intrusion assessment along the Volturno River (Italy) via numerical modelling and spectral analysis. J. Hydrol. 626, 130289. https://doi.org/10.1016/j.jhydrol.2023.130289.
Giambastiani, B.M.S., Kidanemariam, A., Dagnew, A., Antonellini, M., 2021. Evolution of salinity and water table level of the phreatic coastal aquifer of the emilia romagna region (Italy). Water 13 (3), 372. https://doi.org/10.3390/w13030372.
Haque, A., Salama, A., Lo, K., Wu, P., 2021. Surface and groundwater interactions: a review of coupling strategies in detailed domain models. Hydrology 8 (1), 35. https://doi.org/10.3390/hydrology8010035.
Harbaugh, A.W., 2005. MODFLOW-2005, the US Geological Survey Modular Ground-Water Model: The Ground-Water Flow Process; U.S. Geological Survey Techniques and Methods 6-A16; US Department of the Interior; US Geological Survey: Reston, VA, USA, p. 253. https://doi.org/10.3133/tm6A16.
Hilhorst, M.A., 2000. A pore water conductivity sensor. Soil. Sci. Soc. Am. J. 64, 1922–1925. https://doi.org/10.2136/sssaj2000.6461922x.
Hussain, M.S., Abd-Elhamid, H.F., Javadi, A.A., Sherif, M.M., 2019. Management of seawater intrusion in coastal aquifers: a review. Water 11 (12), 2467. https://doi.org/10.3390/w11122467.
Ji, Z.G., 2017. In: Hydrodynamics and Water Quality: Modeling Rivers, Lakes, and Estuaries. John Wiley & Sons. https://doi.org/10.1002/9781119371946.
Kassem, A., Ali, K.E.C., Sefelnasr, A., Sherif, M., 2024. Optimization of pumping and injection regimes for mitigation of seawater intrusion. Resources, Environment and Sustainability 15, 100140. https://doi.org/10.1016/j.resenv.2023.100140.
Klassen, J., Allen, D.M., 2017. Assessing the risk of saltwater intrusion in coastal aquifers. J. Hydrol. 551, 730–745. https://doi.org/10.1016/j.jhydrol.2017.02.044.
Kourgialas, N.N., Dokou, Z., Karatzas, G.P., Panagopoulos, G., Soupios, P., Vafidis, A., Manoutsoglou, E., Schafmeister, M., 2016. Saltwater intrusion in an irrigated agricultural area: combining density-dependent modelling and geophysical methods. Environ. Earth Sci. 75, 1–13. https://doi.org/10.1007/s12665-015-4856-y.
Li, C., Gao, X., Li, S., Bundschuh, J., 2020. A review of the distribution, sources, genesis, and environmental concerns of salinity in groundwater. Environ. Sci. Pollut. Res. 27, 41157–41174. https://doi.org/10.1007/s11356-020-10354-6.
Lionello, P., Scarascia, L., 2018. The relation between climate change in the Mediterranean region and global warming. Reg. Environ. Chang. 18, 1481–1493. https://doi.org/10.1007/s10113-018-1290-1.
Lu, W., Yang, Q., Martín, J.D., Juncosa, R., 2013. Numerical modelling of seawater intrusion in Shenzhen (China) using a 3D density-dependent model including tidal effects. J. Earth Syst. Sci. 122, 451–465. https://doi.org/10.1007/s12040-013-0273-3.
Lyu, P., Song, J., Yin, Z., Wu, J., Wu, J., 2024. Integrated SEAWAT model and GALDIT method for dynamic vulnerability assessment of coastal aquifer to seawater intrusion. Sci. Tot. Environ. 925, 171740. https://doi.org/10.1016/j.scitotenv.2024.171740.
Mastrocicco, M., Busico, G., Colombani, N., Vigliotti, M., Ruberti, D., 2019. Modelling actual and future seawater intrusion in the Variconi coastal wetland (Italy) due to climate and landscape changes. Water 11 (7), 1502. https://doi.org/10.3390/w11071502.
Mastrocicco, M., Colombani, N., 2021. The issue of groundwater salinization in coastal areas of the mediterranean region: a review. Water 13 (1), 90. https://doi.org/10.3390/w13010090.
Matano, F., Sacchi, M., Vigliotti, M., Ruberti, D., 2018. Subsidence trends of Volturno river coastal plain (northern Campania, southern Italy) inferred by SAR interferometry data. Geosciences 8 (1), 8. https://doi.org/10.3390/geosciences8010008.
Meyer, R., Engesgaard, P., Sonnenborg, T.O., 2019. Origin and dynamics of saltwater intrusion in a regional aquifer: combining 3-D saltwater modeling with geophysical and geochemical data. Water Resour. Res. 55, 1792–1813. https://doi.org/10.1029/2018WR023624.
Ntona, M.M., Busico, G., Mastrocicco, M., Kazakis, N., 2022. Modeling groundwater and surface water interaction: an overview of current status and future challenges. Sci. Tot. Environ. 846, 157355. https://doi.org/10.1016/j.scitotenv.2022.157355.
Pappenberger, F., Beven, K., Horritt, M., Blazkova, S.J.J.O.H., 2005. Uncertainty in the calibration of effective roughness parameters in HEC–RAS using inundation and downstream level observations. J. Hydrol. 302 (1–4), 46–69. https://doi.org/10.1016/j.jhydrol.2004.06.036.
Parisi, A., Monno, V., Fidelibus, M.D., 2018. Cascading vulnerability scenarios in the management of groundwater depletion and salinization in semi-arid areas. Int. J. Disaster Risk Reduct. 30, 292–305. https://doi.org/10.1016/j.ijdrr.2018.03.004.
Parizi, E., Hosseini, S.M., Ataie-Ashtiani, B., Simmons, C.T., 2019. Vulnerability mapping of coastal aquifers to seawater intrusion: review, development and application. J. Hydrol. 570, 555–573. https://doi.org/10.1016/j.jhydrol.2018.12.021.
Richardson, C.M., Davis, K.L., Ruiz-González, C., Guimond, J.A., Michael, H.A., Paldor, A., Moosdorf, N., Paytan, A., 2024. The impacts of climate change on coastal groundwater. Nat. Rev. Earth Environ. 5, 100–119. https://doi.org/10.1038/s43017-023-00500-2.
Rodriguez, L.B., Cello, P.A., Vionnet, C.A., Goodrich, D., 2008. Fully conservative coupling of HEC-RAS with MODFLOW to simulate stream–aquifer interactions in a drainage basin. J. Hydrol. 353 (1–2), 129–142. https://doi.org/10.1016/j.jhydrol.2008.02.002.
Ruberti, D., Buffardi, C., Sacchi, M., Vigliotti, M., 2022. The late Pleistocene-Holocene changing morphology of the Volturno delta and coast (northern Campania, Italy): geological architecture and human influence. Quat. Int. 625, 14–28. https://doi.org/10.1016/j.quaint.2022.03.023.
Schiavo, M., Colombani, N., Mastrocicco, M., 2023. Modeling stochastic saline groundwater occurrence in coastal aquifers. Water Res. 235, 119885. https://doi.org/10.1016/j.watres.2023.119885.
Sedighkia, M., Datta, B., 2024. Salinity management of reservoirs by linking hydrodynamic model, surrogate model, and evolutionary optimization. Int. J. Environ. Sci. Technol. 21 (8), 6235–6248.
Seibert, S.L., Greskowiak, J., Bungenstock, F., Freund, H., Karle, M., Meyer, R., Oude Essink, G.H.P., van Engelen, J., Massmann, G., 2023. Paleo-hydrogeological modeling to understand present-day groundwater salinities in a low-lying coastal groundwater system (Northwestern Germany). Water Resour. Res. 59 (4), e2022WR033151. https://doi.org/10.1029/2022WR033151.
Setiawan, I., Morgan, L.K., Doscher, C., 2023. Saltwater intrusion from an estuarine river: a field investigation. J. Hydrol. 617, 128955. https://doi.org/10.1016/j.jhydrol.2022.128955.
Sorgente, R., Di Maio, A., Pessini, F., Ribotti, A., Bonomo, S., Perilli, A., Alberico, I., Lirer, F., Cascella, A., Ferraro, L., 2020. Impact of freshwater inflow from the Volturno river on coastal circulation. Front. Mar. Sci. 7, 293. https://doi.org/10.3389/fmars.2020.00293.
Soudi, M., Ahmadi, H., Yasi, M., Sibilla, S., Fenocchi, A., Hamidi, S.A., 2019. Investigation over the capability of MIKE 3 flow model FM to simulate the hydrodynamics and salinity distribution of hypersaline lakes: lake Urmia (Iran) as case study. Coastal Eng. J. 61 (4), 486–501. https://doi.org/10.1080/21664250.2019.1636474.
Tarallo, D., Alberico, I., Cavuoto, G., Pelosi, N., Punzo, M., Di Fiore, V., 2023. Geophysical assessment of seawater intrusion: the Volturno Coastal Plain case study. Appl. Water. Sci. 13, 234. https://doi.org/10.1007/s13201-023-02033-x.
Tully, K.L., Weissman, D., Wyner, W.J., Miller, J., Jordan, T., 2019. Soils in transition: saltwater intrusion alters soil chemistry in agricultural fields. Biogeochem. 142, 339–356. https://doi.org/10.1007/s10533-019-00538-9.
Turgeon, F., Larocque, M., Meyzonnat, G., Dorner, S., Bourgault, M.A., 2018. Examining the challenges of simulating surface water–groundwater interactions in a post-glacial environment. Can. Water Resour. J. 43 (2), 262–280. https://doi.org/10.1080/07011784.2017.1414635.
Vaux, H., 2011. Groundwater under stress: the importance of management. Environ. Earth Sci. 62, 19–23. https://doi.org/10.1007/s12665-010-0490-x.
Vengosh, A., Helvaci, C., Karamanderesi, Ì.H., 2003. Reply to the comment on "Geochemical constraints for the origin of thermal waters from western Turkey" by Umran Serpen and Tahir Öngür. Appl. Geochem. 18 (7), 1117–1119. https://doi.org/10.1016/S0883-2927(02)00209-3.
Wang, Y., Chen, N., 2021. Recent progress in coupled surface–ground water models and their potential in watershed hydro-biogeochemical studies: a review. Watershed Ecol. Environ. 3, 17–29. https://doi.org/10.1016/j.wsee.2021.04.001.
Yang, J., Graf, T., Herold, M., Ptak, T., 2013. Modelling the effects of tides and storm surges on coastal aquifers using a coupled surface–subsurface approach. J. Contam. Hydrol. 149, 61–75. https://doi.org/10.1016/j.jconhyd.2013.03.002.
Yoon, B.I., Woo, S.B., 2015. The along-channel salinity distribution and its response to river discharge in tidally-dominated Han River Estuary, South Korea. Procedia Eng. 116, 763–770. https://doi.org/10.1016/j.proeng.2015.08.362.
Yu, S., Jiao, J.J., Luo, X., Li, H., Wang, X., Wang, Q., Yao, M., Guo, Y., Deng, Z., Zuo, J., 2023. Vertical leaching of paleo-saltwater in a coastal aquifer-aquitard system of the Pearl River Delta. J. Hydrol. 626, 130168. https://doi.org/10.1016/j.jhydrol.2023.130168.
Yuan, L.R., Xin, P., Kong, J., Li, L., Lockington, D., 2011. A coupled model for simulating surface water and groundwater interactions in coastal wetlands. Hydrol. Process. 25 (23), 3533–3546. https://doi.org/10.1002/hyp.8079.
Zhang, B., Zheng, T., Zheng, X., Jiang, S., Cao, M., Walther, M., Lu, C., 2023. Dynamics of upstream saltwater intrusion driven by tidal river in coastal aquifers. Sci. Tot. Environ. 877, 162857. https://doi.org/10.1016/j.scitotenv.2023.162857.